



UNIVERSITY OF LEEDS

This is a repository copy of *Large Eddy Simulation of Particle Agglomeration with Shear Breakup in Turbulent Channel Flow*.

White Rose Research Online URL for this paper:  
<http://eprints.whiterose.ac.uk/132564/>

Version: Accepted Version

---

**Article:**

Njobuenwu, DO and Fairweather, M (2018) Large Eddy Simulation of Particle Agglomeration with Shear Breakup in Turbulent Channel Flow. *Physics of Fluids*, 30 (6). 063303. ISSN 1070-6631

<https://doi.org/10.1063/1.5037174>

---

© 2018. This article may be downloaded for personal use only. Any other use requires prior permission of the author and AIP Publishing. The following article appeared in *Physics of Fluids* and may be found at <https://doi.org/10.1063/1.5037174>

**Reuse**

Items deposited in White Rose Research Online are protected by copyright, with all rights reserved unless indicated otherwise. They may be downloaded and/or printed for private study, or other acts as permitted by national copyright laws. The publisher or other rights holders may allow further reproduction and re-use of the full text version. This is indicated by the licence information on the White Rose Research Online record for the item.

**Takedown**

If you consider content in White Rose Research Online to be in breach of UK law, please notify us by emailing [eprints@whiterose.ac.uk](mailto:eprints@whiterose.ac.uk) including the URL of the record and the reason for the withdrawal request.



[eprints@whiterose.ac.uk](mailto:eprints@whiterose.ac.uk)  
<https://eprints.whiterose.ac.uk/>

# Large eddy simulation of particle agglomeration with shear breakup in turbulent channel flow

Derrick O. Njobuenwu <sup>a)</sup> and Michael Fairweather

*School of Chemical and Process Engineering, University of Leeds, Leeds, LS2 9JT, UK*

*<sup>a)</sup> Corresponding author: D.O.Njobuenwu@leeds.ac.uk*

A systematic technique is developed for studying particle dynamics as induced by a turbulent liquid flow, in which transport, agglomeration and breakup are considered. An Eulerian description of the carrier phase obtained using large eddy simulation is adopted and fully coupled to a Lagrangian definition of the particle phase using a pointwise discrete particle simulation. An efficient hard-sphere interaction model with deterministic collision detection enhanced with an energy-balance agglomeration model was implemented in an existing computational fluid dynamic code for turbulent multiphase flow. The breakup model adopted allows instantaneous breakup to occur once the transmitted hydrodynamic stress within an agglomerate exceeds a critical value, characterised by a fractal dimension and the size of the agglomerate. The results from the developed technique support the conclusion that the local turbulence kinetic energy, its dissipation rate and the agglomerate fractal dimension control the kinetics of the agglomeration and de-agglomeration processes, and as well as defining with time the morphology of the particles and their resultant transport. Overall, the results are credible and consistent with the expected physical behaviour and with known theories.

## I. INTRODUCTION

Turbulent solid-liquid flows are encountered in numerous natural, industrial and biomedical processes. Our interest is in the prediction of particle transport with a physically-sound description of both particle-particle interactions (e.g. collision and agglomeration) and fluid-particle interactions (e.g. breakup). In addition, particle-wall interactions may occur leading to wall deposition, wall erosion or particle re-suspension depending on the magnitude of the short-range particle-surface interactions <sup>1</sup>. These multiscale particle interactions (with the wall, other particles and the fluid) define with time the morphology of the particles and their resultant transport within the system, as well as any turbulence modulation <sup>2</sup> of the carrier phase. The general description of the multiscale interaction of the dispersed phase with the

turbulent fluid flow is a challenging task, however, due to inherent nonlinearities, inhomogeneities and coupling over disparate temporal and spatial scales <sup>3,4</sup>.

In most systems, there is competition between agglomeration and breakup. Agglomeration is greatly enhanced by the way individual particles interact with turbulence structures, and in particular due to their segregation into regions of strain where they either breakup through the high shearing of the flow or continue to grow with enhanced collision rates <sup>5,6</sup>. The rate of agglomeration and breakup in pumps and in pipe flow, for example, are important flow characteristics that feed into transport prediction models used in industry <sup>7</sup>.

For predicting and investigating particle transport, agglomeration and breakup, computational fluid dynamic (CFD) methods have been developed, alongside advanced experimental approaches. It is important that numerical simulations replicate actual physical experiments in order to improve confidence in their use in practical applications. However, detailed experimental data for wall-bounded turbulent multiphase flows is scarce, and what is available is often incomplete, and hence unsuitable for the thorough validation of numerical simulations. In addition, particle-fluid and particle-particle interaction-related simulations are very difficult to validate given the inherent difficulties in measuring such phenomena experimentally. To overcome these challenges, the numerical methods underlying the simulation approaches adopted must be carefully selected and assessed to improve the integrity of the simulations and the findings that result therefrom. In addition, and in the absence of appropriate experimental data for model validation, efforts must be made to ensure that simulations are qualitatively correct as a first necessary step in ensuring their quantitative accuracy.

One of the main CFD tools being used to underpin the understanding of turbulent flows is direct numerical simulation (DNS). Several established methods have been developed for simulating the transport of the dispersed phase in turbulent two-phase flows in conjunction with DNS, including

pointwise particle tracking <sup>8</sup>, interface tracking <sup>9</sup> and the lattice Boltzmann method <sup>10</sup>. Each of these methods has its limitations in terms of its robustness and its numerical accuracy and efficiency. Numerical complexity also limits the DNS of turbulent multiphase flows to small Reynolds number ( $Re_\tau \leq 590$ ), e.g. <sup>11, 12</sup>. DNS of a turbulent channel flow (single phase) up to  $Re_\tau \approx 5200$  has appeared recently <sup>13</sup>. However, because of the presence of complex physical phenomena interacting with turbulence (multiphase flow, inter-particle collision, complex geometries) and the fact that the Reynolds number of industrial scale flows is a few orders of magnitude larger than is currently achievable, the use DNS in general is not feasible <sup>4</sup>.

Large eddy simulation (LES) has been adopted to study industrial and natural flow applications, and for the study of complex physics. LES with modelling of the sub-grid scale (SGS) and of the SGS influence on particle dispersion can reproduce the results of DNS and experiment with reasonable accuracy and computational efficiency for turbulent particle-laden flow. Recently, Schutte *et al.* <sup>14</sup> have demonstrated that the properties of the agglomerates formed in such flows change when two-way coupling between the discrete and continuous phases is considered rather than one-way coupling. The authors further reported that no significant difference was observed in the properties of the agglomerates formed based on results obtained using LES or DNS. The work of Schutte *et al.* <sup>14</sup> therefore shows that eddy-resolving simulations (LES and DNS) can successfully capture particle-particle and particle-turbulence interactions.

To model inter-particle collision and agglomeration using a microscopic approach, both the hard-sphere and soft-sphere collision models can be used. LES coupled to the hard-sphere collision model <sup>15-17</sup> and energy-balanced and momentum-balanced agglomeration models <sup>4, 18-20</sup> have been used to study inter-particle collision and particle agglomeration in turbulent channel flow. Afkhami *et al.* <sup>21</sup> and Hellestø *et al.* <sup>22</sup> applied LES coupled to the discrete element method based on the soft-sphere collision model <sup>23</sup> to

model particle agglomeration in solid-liquid turbulent channel flow. Ho and Sommerfeld <sup>24</sup>, and Sommerfeld and Stübing <sup>25</sup>, also used a macroscopic approach to model particle agglomeration processes in homogeneous isotropic turbulence based on stochastic collision model <sup>26</sup>.

Agglomeration is favoured when the cohesive force between particles is stronger than the kinetic energy between colliding particles <sup>18</sup>. Once formed, the individual agglomerates can interact with turbulent structures which may cause them to segregate into straining regions where they either breakup through the high shearing of the flow in these regions or continue to grow with enhanced collision rates <sup>6</sup>. Stresses passed from the turbulent flow to the agglomerates are induced by shear stress from fluid flow, particle-particle and particle-wall collisions <sup>7, 27, 28</sup>. Agglomerates breakup when the hydrodynamic stresses exceed a critical stress which characterises the agglomerate's strength <sup>28-30</sup>.

Particles collide by different mechanisms and stick together forming irregular-shaped or fractal-like <sup>7, 30</sup>. The structure of these agglomerates is characterised by the fractal dimension,  $d_f$ , and pre-exponential factor,  $k_n$ , of simulated agglomerates of monodisperse primary particles for ballistic or diffusion-limited particle-agglomerate and agglomerate-agglomerate collision mechanisms <sup>31</sup>. Rector and Bunker <sup>7</sup> in studying how colloidal particles in sludge suspensions interaction with each other have shown that the primary particle size, agglomerate diameter and the fractal dimension of the agglomerate influence many of the key sludge properties, such as viscosity, sedimentation rate, and sediment density. Inci *et al.* <sup>32</sup> used Langevin dynamics to investigate the aggregation of soot nano-particles in turbulent flows, with the morphology of the aggregates again characterised by the fractal dimension,  $d_f$ . The fractal dimension of agglomerates formed by diffusion-limited agglomerate-agglomerate agglomeration is typically 1.78, and for diffusion-limited particle-agglomerate agglomeration  $d_f = 2.5$ , for ballistic agglomerate-agglomerate agglomeration  $d_f = 1.90$ , and for ballistic particle-agglomerate agglomeration  $d_f = 3.0$ , as reviewed by Eggersdorfer and Pratsinis <sup>31</sup>. The use of  $d_f$  to characterize agglomerates has become standard practice

even though such particles may not fully obey fractal theory, but they are considered to be sufficiently close to it to be judged fractal-like. Therefore, our interest is in how the fractal dimension influences agglomerate breakup and, subsequently, particle collision and agglomeration processes.

Contrary to previous collision only <sup>17</sup>, agglomeration only <sup>4, 18-21</sup> and breakup only <sup>27, 29, 33, 34</sup> studies, or studies based on phenomenological approaches (e.g. population balance equation) <sup>35</sup>, the present work investigates both particle agglomeration and breakup in order for the predictive technique employed to be applicable to practical processes. In this paper, therefore, we investigate the competition between agglomeration and breakup using a previously well-validated LES <sup>36</sup> coupled to a discrete particle simulation (DPS) <sup>4</sup>, an energy-balanced agglomeration model <sup>18</sup> and a shear-induced agglomerate breakup approach <sup>33, 37</sup>. The adopted breakup model has been implemented by Babler *et al.* <sup>29</sup> for estimation of the breakup rate of small aggregates in fully developed bounded and unbounded turbulence, and by Marchioli and Soldati <sup>34</sup> for the breakup of ductile agglomerates. This study is motivated by the fact that agglomeration and breakup define with time the morphology of the particles, and the transport and settling dynamics of particle suspensions and sludges encountered in nuclear waste treatment. The techniques proposed in this paper are, however, fundamental and generic and can be applied to particle agglomeration and agglomerate breakup under aerodynamic and hydrodynamic conditions that occur in various other industrial and natural processes.

## II. MATHEMATICAL MODEL

### A. Large Eddy Simulation

In large eddy simulation, the filtered governing equations of mass and momentum of an incompressible flow, with the contribution of the dispersed phase included, can be written as:

$$\frac{\partial \bar{u}_i}{\partial x_i} = 0 \quad (1)$$

$$\frac{\partial \bar{u}_i}{\partial t} + \bar{u}_j \frac{\partial \bar{u}_i}{\partial x_j} = -\frac{1}{\rho} \frac{\partial \bar{p}}{\partial x_i} + \frac{\partial \bar{\tau}_{ij}}{\partial x_j} - \frac{\partial \tau_{ij}^{sgs}}{\partial x_j} + \bar{f}_i + \Pi \delta_{i3} \quad (2)$$

where  $\rho$ ,  $u$  and  $p$  represent the fluid density, velocity and pressure, respectively. The tensors  $\bar{\tau}_{ij}$  and  $\tau_{ij}^{sgs}$  are the viscous stress and the unknown sub-grid scale (SGS) stress tensors. The SGS stress tensor, defined as  $\tau_{ij}^{sgs} = \overline{u_i u_j} - \bar{u}_i \bar{u}_j$ , is closed using the dynamically calibrated version of the Smagorinsky model<sup>38,39</sup>, where the anisotropic part of the SGS stress is related to the filtered rate of strain tensor via  $\tau_{ij}^{sgs} = 2\nu_{sgs} \bar{S}_{ij}$  with the SGS kinematic viscosity given by  $\nu_{sgs} = C_S \Delta^2 \|\bar{S}_{ij}\|$ .  $C_S$  is the Smagorinsky constant and  $\|\bar{S}_{ij}\|$  represents a Frobenius norm  $\|\bar{S}_{ij}\| = (2\bar{S}_{ij}\bar{S}_{ij})^{1/2}$  of the filtered rate of strain tensor,  $\bar{S}_{ij} = 1/2 (\partial \bar{u}_j / \partial x_i + \partial \bar{u}_i / \partial x_j)$ . The dynamic version of the Smagorinsky model<sup>38,39</sup>, allows the value of the parameter  $C_S$  to be determined as a function of time and position,  $C_S = C_S(x_i, t)$ . Coupling between the fluid and particle phases is incorporated by the addition of a momentum source,  $\bar{f}_i$ . The momentum source term is evaluated from  $\bar{f}_i = (1/\Delta^3) \sum_{p=1}^{N_p} S_i(p)$ , where the summation is performed over the number of particles present within a specific control volume, and  $\Delta = (\Delta_x \times \Delta_y \times \Delta_z)^{1/3}$  is the filter width and  $S_i(p)$  is the momentum source term arising from the  $p^{th}$  particle. In this paper, the contribution of the SGS stress momentum exchange was not accommodated. The source term  $\Pi \delta_{i3}$  is the mean pressure gradient imposed that drives the flow and  $\delta_{ij}$  is the Kronecker function ( $\delta_{ij} = 1$  for  $i = j$ ,  $\delta_{ij} = 0$  for  $i \neq j$ ).

## B. Discrete Particle Simulation

The discrete particle motion is governed by the following Lagrangian equations:

$$d\mathbf{v} = \left\{ \frac{(\bar{\mathbf{u}} - \mathbf{v})}{\tau_p} f_D + C_{SL} \frac{3\rho}{4\rho_p} [(\bar{\mathbf{u}} - \mathbf{v}) \times \bar{\boldsymbol{\omega}}] + \frac{\rho}{\rho_p} \frac{D\bar{\mathbf{u}}}{Dt} + \frac{\rho}{2\rho_p} \left( \frac{d\bar{\mathbf{u}}}{dt} - \frac{d\mathbf{v}}{dt} \right) \right\} dt + \left( C_0 \frac{k_{sgs}}{\tau_t} \right)^{0.5} d\mathbf{W}_t \quad (3)$$

$$d\mathbf{x}_p = \mathbf{v} dt, \quad (4)$$

where the derivatives  $d/dt$  and  $D/Dt$  represent Lagrangian derivatives following the particle and the fluid element, respectively, and bold symbols denote vector quantities, with  $d\bar{\mathbf{u}}/dt = \partial\bar{\mathbf{u}}/\partial t + \mathbf{v} \cdot \nabla\bar{\mathbf{u}}$  and  $D\bar{\mathbf{u}}/Dt = \partial\bar{\mathbf{u}}/\partial t + \bar{\mathbf{u}} \cdot \nabla\bar{\mathbf{u}}$ . The terms on the right-hand side of Eq. (3) are, respectively, contributions from the drag, shear lift, pressure-gradient, and added-mass forces, and a stochastic force term accounting for the influence of the SGS fluid velocity fluctuations on particle acceleration<sup>36</sup>. Gravity and buoyancy forces were not included as the focus of this paper is limited to turbulence effects on collision, agglomeration and breakup events.  $\mathbf{v}$  and  $\mathbf{x}_p$  are the particle instantaneous velocity and position, and  $\bar{\mathbf{u}}$  and  $\bar{\boldsymbol{\omega}} = 0.5(\nabla \times \bar{\mathbf{u}})$  are known resolved fluid velocities and rotation interpolated at the particle position. The terms  $f_D$  and  $C_{SL}$  are, respectively, the drag and shear lift forces taken from the Schiller and Naumann drag correlation and the Mei<sup>40</sup> shear lift force correlation, both due to the particles' finite Reynolds number.

For the stochastic term,  $C_0 = 1$  is a dispersion coefficient<sup>36</sup> and the unresolved turbulence kinetic energy,  $k_{sgs} = 2\Delta^2 C_S^{2/3} \bar{S}_{ij} \bar{S}_{ij}$ , of the continuous phase is computed assuming equilibrium of the small scales. The Smagorinsky constant,  $C_S = C_S(\mathbf{x}, t)$ , is closed using the dynamic calibration of the Smagorinsky model constant<sup>38,39</sup>, with the filter width  $\Delta$  and the filtered strain tensor  $\bar{S}_{ij}$  as defined in the previous subsection. The term  $d\mathbf{W}_t = \boldsymbol{\xi} \times \sqrt{dt}$  is an incremental Wiener term, where  $\boldsymbol{\xi}$  is a random vector sampled with zero mean and a variance of unity, independently for each time step.. The interaction between particles and the fluid phase turbulence is considered using the following time scale,  $\tau_t = \tau_p$ . Other alternative time scales are reported in Bini and Jones<sup>36</sup>.

### C. Particle Collisions

Particle-particle interaction is modelled using the deterministic hard-sphere collision model assuming binary collisions and neglecting particle angular momentum. The concept of virtual cells<sup>16</sup> is adopted, where the computational domain is decomposed into  $d_x \times d_y \times d_z$  virtual cells. The standard

deterministic collision detection procedure is limited to the particles in each virtual cell. The use of the concept of virtual cells enables the cost of checking for collisions to be reduced from  $O(N_0^2)$ , when collisions between all possible particle pairs are considered, to  $O(N_0)$ .

In order for two particles within a virtual cell to collide, two conditions have to be fulfilled<sup>16</sup>. The first condition is that they must approach each other, expressed as  $(\mathbf{x}_r \cdot \mathbf{v}_r < 0)$ , where  $\mathbf{x}_r$  and  $\mathbf{v}_r$  are the relative separation distance and relative velocity between the two particles, respectively. The second condition is that the minimum separation distance,  $\mathbf{x}_{r,\min}$ , occurring at  $\Delta t_{\min}$  within a time step,  $\Delta t$ , must be less than the sum of the particles radii,  $d_{12} = (d_{p,1} + d_{p,2})/2$ . Therefore, contacts between neighbouring particles within a time step are detected by satisfying the conditions<sup>16</sup>:

$$(\mathbf{x}_r \cdot \mathbf{v}_r < 0) \ \& \ (|\mathbf{x}_{r,\min}| \leq d_{12}) \ \text{and} \ (\Delta t_{\min} \leq \Delta t) \quad (5)$$

If a collision is detected, the position and velocity vectors of the colliding particles are updated as per the hard-sphere model.

#### D. Particle Agglomeration

Agglomeration of the colliding particles is based on an expression which permits agglomeration if the elastic energy (i.e. the relative kinetic energy before the collision minus the dissipated energy) after the compression period of the collision is less than the work required to overcome the van der Waals forces<sup>18</sup>:

$$\frac{(\mathbf{v}_2^- - \mathbf{v}_1^-)^2 - [(\mathbf{v}_2^- - \mathbf{v}_1^-) \cdot \mathbf{n}_c]^2(1 - e_n^2)}{|\mathbf{v}_2^- - \mathbf{v}_1^-| \cdot \mathbf{n}_c} \leq \frac{H^*}{6\delta_0^{*2}} \left[ (1 - e_n^2) \frac{6}{\pi^2 \rho_p^* \bar{p}^*} \frac{d_{p,1}^{*3} + d_{p,2}^{*3}}{d_{p,1}^{*2} d_{p,2}^{*2} (d_{p,1}^* + d_{p,2}^*)} \right]^{1/2} \quad (6)$$

where quantities with the superscript \* are made dimensionless in the integral scale using the channel half-height,  $h$ , fluid bulk velocity,  $u_b$ , and fluid density,  $\rho$ .  $H$  is the particle Hamaker constant,  $\bar{p}$  is the maximum contact pressure at which plastic deformation occurs,  $\delta_0$  is the minimal contact distance and  $e_n$

is the normal restitution coefficient. Note the superscript (–) denotes quantities before the collision, and the subscripts 1 and 2 denote particles number one and two. The agglomerate size,  $d_{p,3}$ , and structure are based on a volume-equivalent sphere,  $d_{p,3} = (d_{p,1}^3 + d_{p,2}^3)^{1/3}$ .

### E. Agglomerate Breakup

Breakup is defined as a singular event in time, i.e. there is an exact moment in time when an agglomerate turns from being intact into being broken. We assume that this happens when the local hydrodynamic stress  $\sigma \sim \mu(\epsilon/\nu)^{1/2}$ , i.e. the applied breaking force at the agglomerate position acting on the agglomerate, exceeds a critical stress,  $\sigma_{cr}$ <sup>29</sup>, i.e. the mechanical strength of the agglomerate. Here,  $\epsilon = 2(\nu + \nu_{sgs})\bar{S}_{ij}\bar{S}_{ij}$  is the instantaneous turbulence kinetic energy dissipation rate at the position of the agglomerate, and  $\mu$  and  $\nu$  are the dynamic and kinematic viscosities, respectively. The critical stress  $\sigma_{cr}$  is a characteristic of the considered agglomerate, i.e.  $\sigma_{cr}$  is a function of the aggregate properties such as size, structure, type of the constituent particles, and the chemical environment. Among these variables, the size of the aggregate is the most crucial. A large body of experimental, numerical and theoretical studies, see Babler *et al.*<sup>29</sup> and cited references, suggest a power law dependency of the form:

$$\sigma_{cr} \sim r^{-q} = N_{pp}^{-q/d_f} \quad (7)$$

where  $N_{pp} \sim r^{d_f}$  is the number of primary particles constituting the agglomerate,  $d_f$  is the agglomerate fractal dimension,  $r$  is the radius of the primary particle, and  $q = [9.2(3 - d_f) + 1]/2$  is a scaling exponent that depends on the agglomerate structure<sup>29</sup>. There are no exact models to effect breakup, and recent research<sup>29</sup> has been limited to detecting the moment break-up events are likely to occur. We adopt this model for detecting breakup events for small agglomerates and subsequently breakup the parent agglomerate into two smaller particles. This method of breaking an agglomerate into two parts is a popular modelling assumption adopted mainly because of the lack of data for other types of breakup mode.

### III. NUMERICAL SIMULATIONS

The simulation treats the continuous phase in an Eulerian framework based on large eddy simulation, using the BOFFIN (Boundary Fitted Flow Integrator) LES code <sup>41</sup>. BOFFIN is a block-structured and boundary conforming coordinate code parallelised by domain decomposition using message passing interface routines. It comprises a second-order accurate finite-volume method, based on an implicit low-Mach-number formulation using a co-located storage arrangement. For the momentum equation convection terms, an energy-conserving discretisation scheme is used, and all other spatial derivatives are approximated by standard second-order central differences. Time derivatives are approximated by a three-point backward difference scheme with variable time step to ensure that the maximum Courant number, based on the filtered velocity, always lies between 0.1 and 0.2. This LES solver has been validated thoroughly for many different flows, e.g. <sup>42, 43</sup>. In this paper, we extend the BOFFIN code to handle four-way coupling with deterministic collision, agglomeration and shear-induced breakup of solid particles.

We simulate a turbulent channel flow at  $Re_\tau = 300$  for validation purposes and at  $Re_\tau = 590$  for the particle agglomeration and agglomerate breakup cases. We adopt  $x$ -,  $y$ - and  $z$ -axes as the wall-normal, spanwise and streamwise directions, respectively. The dimensions of the computational domains and mesh resolution are given in Table 1. For the DPS validation, we matched the parameters used for the DNS at  $Re_\tau = 300$  and density ratio,  $\rho_p/\rho \sim 790$ , employed by Marchioli and Soldati <sup>44</sup>. Two particle sets were considered, characterised by different non-dimensional relaxation times,  $\tau_p^+$ , in a one-way coupled simulation, as listed in Table 2. For the DPS in the  $Re_\tau = 590$  case, a total number  $N_0 = 2,747,570$  of spherical primary calcite particles of diameter  $d_p = 60 \mu m$ , a simulant representative of UK legacy waste sludge, at volume fraction  $\alpha_p = 10^{-3}$  was used, with the mechanical properties for this simulation listed in **Table 3**<sup>24, 46</sup>. In all the simulation cases, periodic boundary conditions were applied in the spanwise

and streamwise directions for both the continuous and dispersed phases. The no-slip condition and perfect elastic wall conditions were imposed on the walls for the continuous and dispersed phases, respectively.

**Table 1:** Grid parameters for LES of turbulent channel flow.  $L_{x(y,z)}$ ,  $N_{x(y,z)}$  and  $\Delta_{x(y,z)}^+$  are the size of the domain, the number of grid points and filter widths in wall units, respectively. Grid parameters used for DNS at  $Re_\tau = 300$  by Marchioli and Soldati <sup>44</sup> and  $Re_\tau = 590$  by Moser *et al.* <sup>45</sup> are also provided for reference.

$Re_\tau$	$L_x \times L_y \times L_z$	$N_x \times N_y \times N_z$	$\Delta_x^+$	$\Delta_y^+$	$\Delta_z^+$
Current LES					
300	$2h \times \pi h \times 2\pi h$	$129 \times 128 \times 128$	0.14 – 14.2	14.84	29.68
590	$2h \times \pi h \times 2\pi h$	$129 \times 128 \times 128$	0.26 – 26.39	29.19	58.38
DNS					
300	$2h \times 2\pi h \times 4\pi h$	$257 \times 256 \times 256$	0.02 - 3.68	7.39	14.78
590	$2h \times \pi h \times 2\pi h$	$257 \times 384 \times 384$	0.04 - 7.20	4.80	9.70

**Table 2:** Particle parameters for validation at  $Re_\tau = 300$ .

$\tau_p^+$	$\tau_p$ (s)	$d_p^+$	$d_p$ ( $\mu\text{m}$ )	$\rho_p/\rho$
1	$1.13 \times 10^{-3}$	0.153	20.4	790
25	$2.83 \times 10^{-2}$	0.765	102.0	790

**Table 3:** Particle (calcite) mechanical properties and associated parameters used in studying particle agglomeration and breakup for the  $Re_\tau = 590$  case.

Parameter	Symbol	Units	Value
Particle density	$\rho_p$	$\text{kg m}^{-3}$	2710
Hamaker constant	$H$	J	$3.8 \times 10^{-20}$
Mean yield stress	$\bar{\sigma}$	Pa	$3.0 \times 10^8$
Minimal contact distance	$\delta_0$	m	$2.0 \times 10^{-10}$
Primary particle diameter	$d_p$	$\mu\text{m}$	60

Normal restitution coefficient	$e_n$	-	0.4
Particle volume fraction	$\alpha_p$	-	$1.0 \times 10^{-3}$
Agglomerate fractal dimension	$d_f$	-	2.0, 2.5, 2.8, 3.0

The particle equations of motion, Eqs. (3) and (4), were integrated using a fourth-order Runge-Kutta scheme. Sixth-order Lagrangian polynomial and trilinear interpolation schemes<sup>47</sup> were used to obtain the fluid properties at a particle's position for the  $Re_\tau = 300$  and  $Re_\tau = 590$  cases, respectively. The particle's initial position was random, and the initial velocity was set equal to that of the fluid at the particle's position. The particles' trajectories were tracked, including inter-particle collisions, for  $t^* > 5000$  to allow for proper mixing before particle agglomeration and breakup were allowed to occur. The time counter was readjusted to  $t^* = 0$  at the start of the particle agglomeration and breakup computation.

The agglomeration kinetics, as illustrated in **Fig. 1(a)**, are such that during the agglomeration process two primary particles (monomers,  $N_{a,i=1}$ ) collide and agglomerate to form a dimer,  $N_{a,i=2}$ , while a monomer and a dimer collide to form a trimer,  $N_{a,i=3}$ , which is an agglomerate of three primary particles, and so on. The breakup kinetics, as illustrated in **Fig. 1(b)**, are in direct opposition to that of agglomeration, such that a trimer breaks up into a monomer and a dimer, and so on.

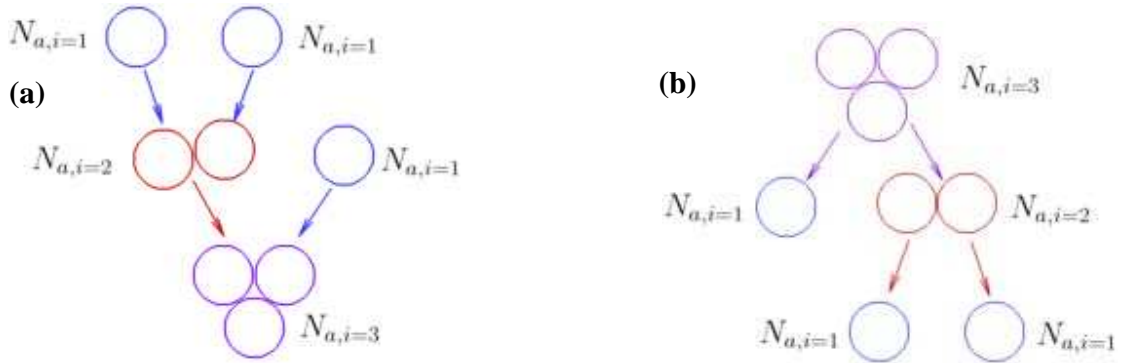


**Fig. 1:** Schematics of **(a)** particle agglomeration process and **(b)** agglomerate breakup process.

Throughout this paper, the velocity, length and time scales are made dimensionless using either wall variables as  $u^+ = u/u_\tau$ ,  $x^+ = xu_\tau/\nu$  and  $t^+ = tu_\tau^2/\nu$ , or using integral scales as  $u^* = u/u_b$ ,  $x^* = x/h$ , and  $t^* = tu_b/h$ .

## IV. RESULTS AND DISCUSSION

### A. Validation of Fluid and Particle Velocity Statistics

Turbulence properties are characterised by the turbulence kinetic energy, with its SGS component,  $k_{sgs}$ , shown in **Fig. 2(a)**. It represents the intensity of the fluid fluctuation velocity. The turbulence kinetic energy dissipation rate,  $\epsilon$ , shown in **Fig. 2(b)**, determines the intensity of the turbulence shear gradient, turbulent length and time scales. The turbulence properties have a significant influence on the particle transport, agglomeration and breakup processes. The turbulence kinetic energy facilitates collisions amongst particles<sup>20</sup>, a precursor to particle agglomeration. while its dissipation rate induces breakup of the formed agglomerates<sup>29</sup>. This makes it imperative to ensure that the solid-liquid flow simulation is validated.

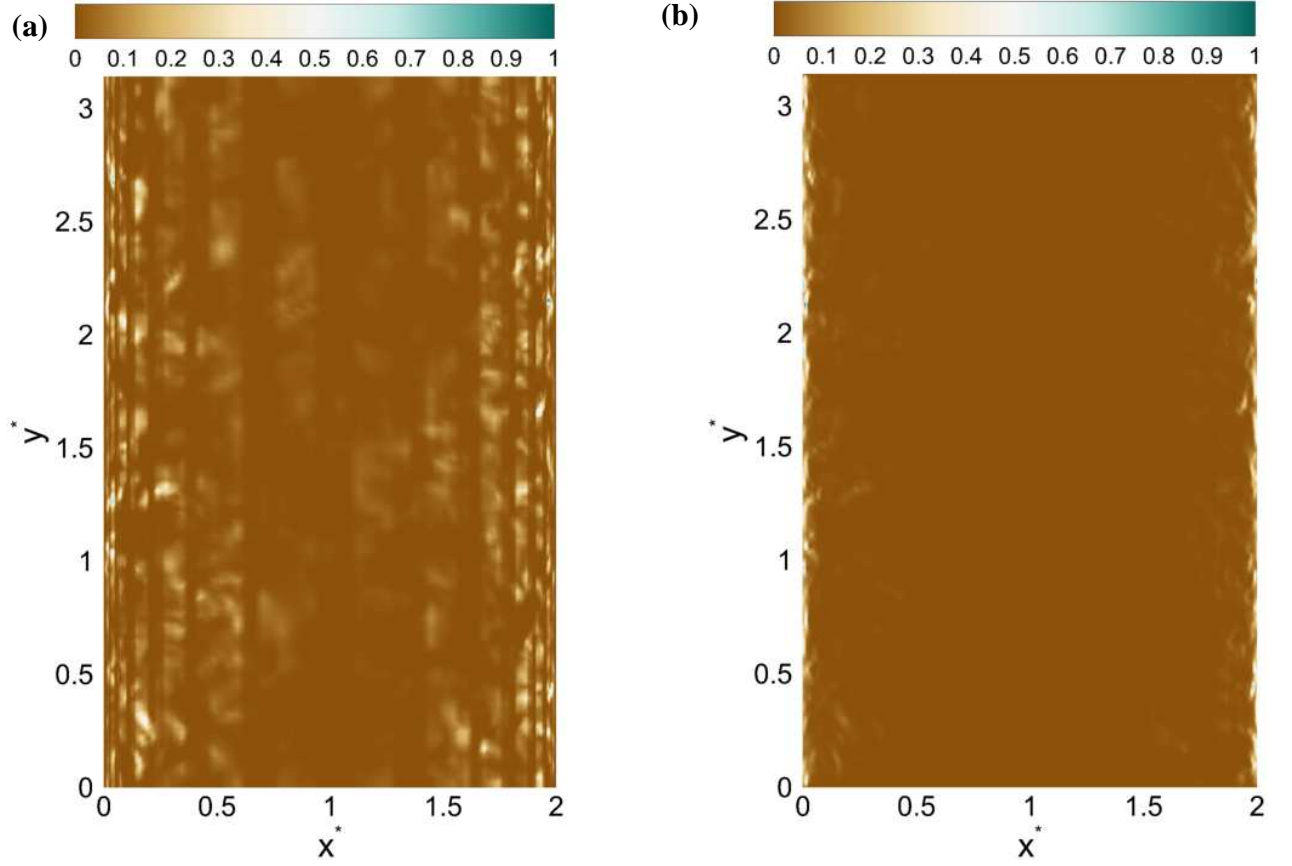


**Fig. 2:** Instantaneous contours on an  $x^* - y^*$  plane: (a) non-dimensional SGS turbulence kinetic energy,  $k_{sgs}/k_{sgs,max}$ , and (b) non-dimensional turbulence kinetic energy dissipation rate,  $\epsilon/\epsilon_{max}$ , for  $Re_\tau = 590$ , sliced at  $z^* \sim 4.6$ .

The computed statistics of the mean streamwise velocity,  $\langle u_z^+ \rangle$ , of the root mean square values of the velocity fluctuations along the wall-normal,  $\langle u_x'^+ \rangle$ , spanwise,  $\langle u_y'^+ \rangle$ , and streamwise,  $\langle u_z'^+ \rangle$ , directions, and of the  $x - z$  component of the Reynolds shear stress,  $\langle u_x'^+ u_z'^+ \rangle$ , are shown in **Fig. 3**. Note that the statistics presented here were gathered for over  $10H/u_\tau$  containing samples taken after each time step ( $\Delta t \sim 3.0 \times 10^{-4}$  s for  $Re_\tau = 300$  and  $\Delta t = 3.5 \times 10^{-4}$  s for  $Re_\tau = 590$ ). The 10 cycles mentioned here refers only to the sampling interval for the fluid and particle velocity statistics presented in Figs. 3 and 4 and not to the agglomeration and breakup events to be described in later sections. This time interval ( $10H/u_\tau$ ) is more than enough to obtain a statistically steady state result. The results are time- and space-averaged (denoted by  $\langle \dots \rangle$ ) as well as averaged over the two halves of the channel, to increase the reliability of the

statistical sample. These statistical moments from the present LES are compared with DNS results for a turbulent channel flow at  $Re_\tau = 300$  <sup>44</sup>, in **Fig. 3(a, b)**, and at  $Re_\tau = 590$  <sup>45</sup>, in **Fig. 3(c,d)**, with good agreement found.

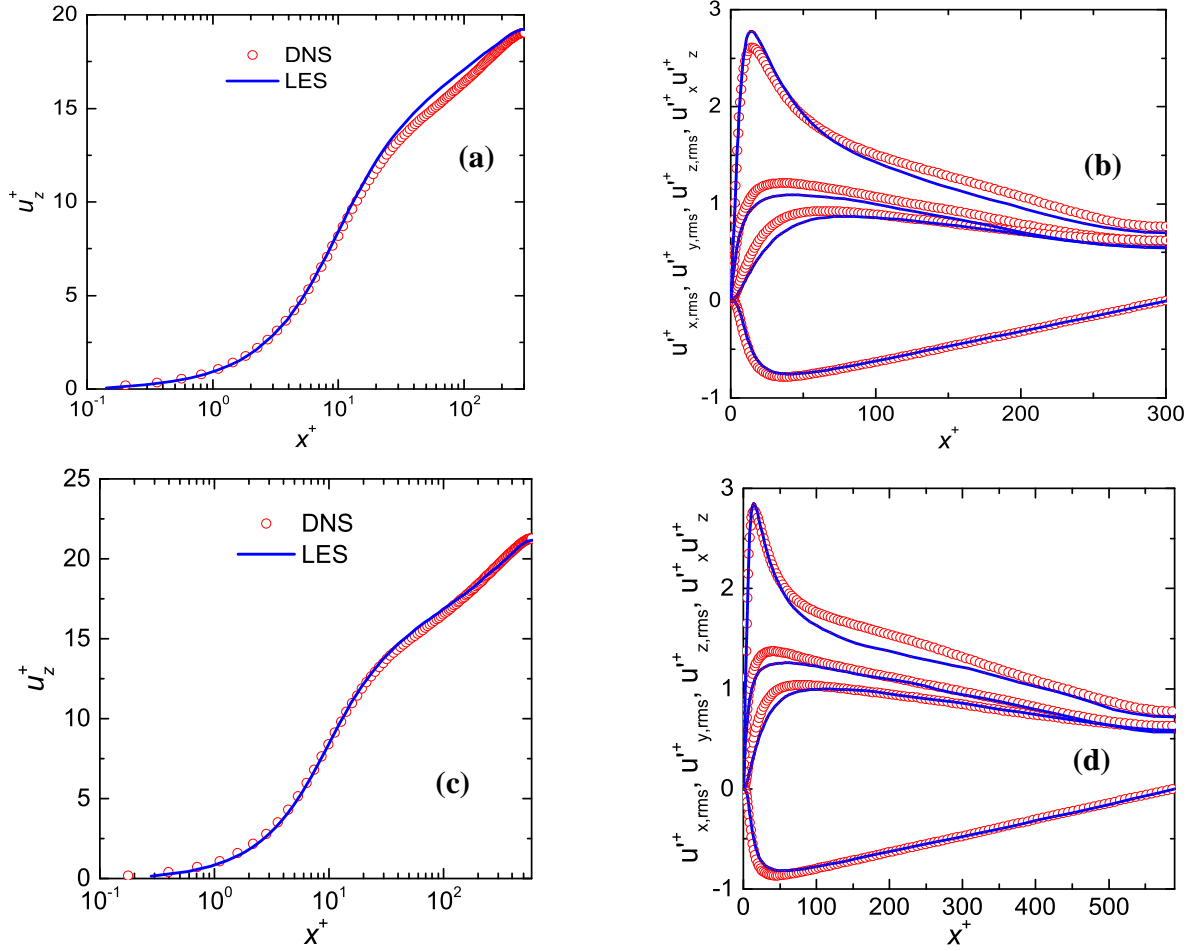


**Fig. 3:** Statistics of fluid phase in turbulent channel flow simulations: (a, c) mean streamwise velocity,  $\langle u_z^+ \rangle$ , and (b, d) root mean square of velocity fluctuations along wall-normal,  $\langle u_x'^+ \rangle$ , spanwise,  $\langle u_y'^+ \rangle$ , and streamwise,  $\langle u_z'^+ \rangle$ , directions, and Reynolds shear stress,  $\langle u_x'^+ u_z'^+ \rangle$ . Simulations at  $Re_\tau = 300$  (a, b) and  $Re_\tau = 590$  (c, d).

Similarly, the velocity profiles of the particles at Stokes numbers  $\tau_p^+ = 1$  and 25 are compared with equivalent values obtained from the DNS database of Marchioli and Soldati <sup>44</sup> at  $Re_\tau = 300$  in **Fig. 4**. As previously reported in Njobuenwu and Fairweather <sup>4</sup>, the comparisons show very good agreement,

confirming that the use of a highly resolved LES and dynamic modelling of the SGS term gives reliable results. Note that the results shown in Figs. (3) and (4) have appeared in an earlier paper<sup>4</sup> and are reproduced here for completeness.

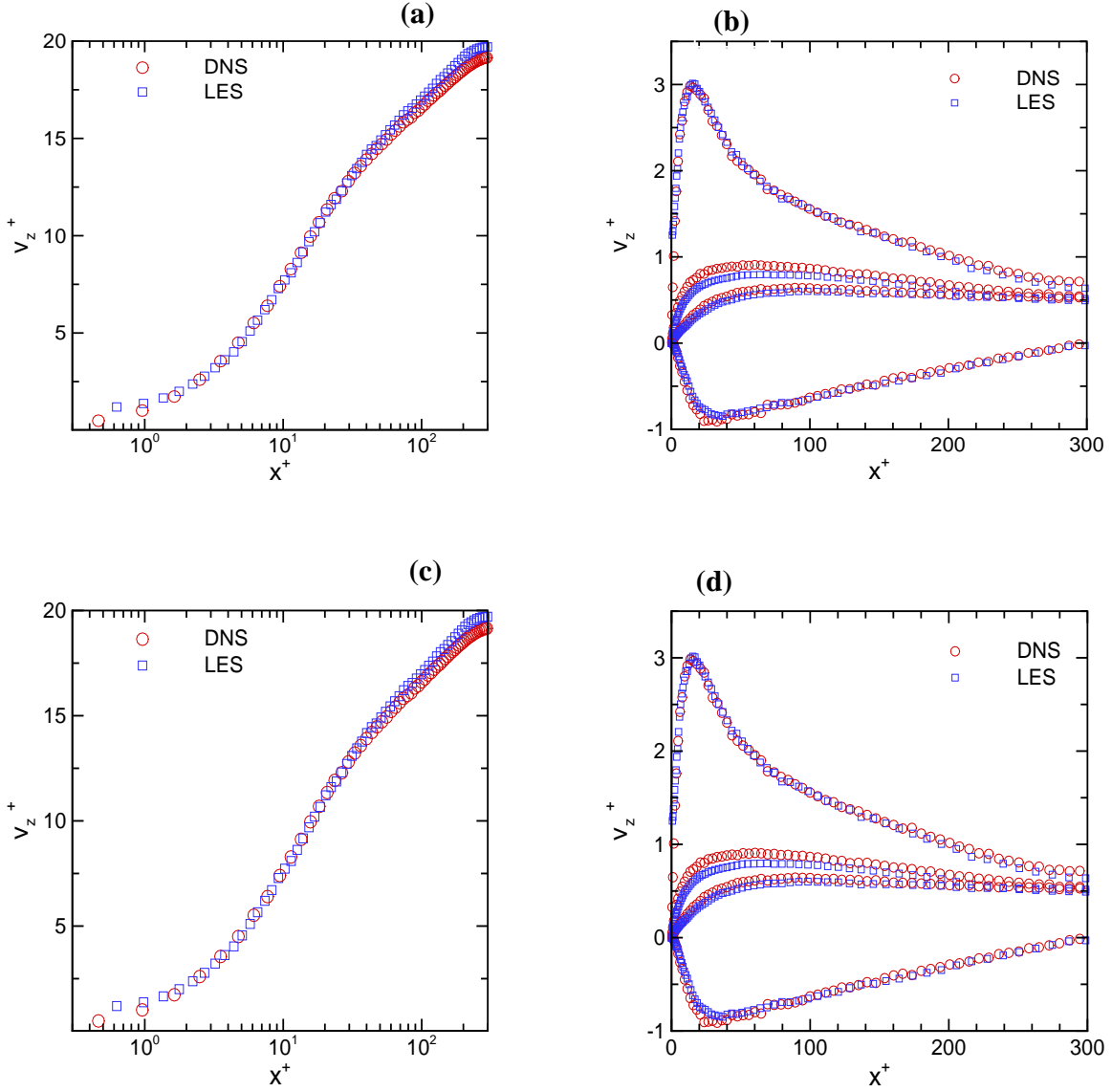


**Fig. 4:** Statistics of particle phase in turbulent channel flow simulations at  $Re_\tau = 300$  with density ratio,  $\rho_p/\rho \sim 790$ : (a, c) mean streamwise velocity, ( $v_z^+$ ), and (b, d) root mean square of velocity fluctuations along wall-normal, ( $v_{x,rms}^+$ ), spanwise, ( $v_{y,rms}^+$ ), and streamwise, ( $v_{z,rms}^+$ ), directions, and Reynolds shear stress, ( $v_x^+ v_z^+$ ). Simulations for (a, b)  $\tau_p^+ = 1$ , and (c, d)  $\tau_p^+ = 25$ .

## B. Particle-Particle Interactions and Agglomerate Breakup

To examine the extent to which the agglomerate fractal dimension,  $d_f$ , during agglomerate breakup influences the global agglomeration process, as well as the transient and steady-state behaviour of the system, a series of simulations were carried out. The work of Soos *et al.*<sup>30</sup> was considered, which reported that agglomeration of solid primary particles in a typically random process results in agglomerate structures with fractal dimensions around 2.0. Under flow conditions, the authors reported that the value of the fractal dimension can be significantly larger, even up to its threshold value of 3.0, due to the restructuring and breakage processes. Hence, in this work, the values of  $d_f$  were set to  $d_f = 2.0, 2.5, 2.8$  and 3.0. A fifth simulation, used as a control, is the case of no-breakup in which case  $d_f \rightarrow \infty$ . All other parameters such as fluid properties and particle properties were kept constant at the values listed in **Tables 1 and 3**. Note that the results for particle agglomeration and breakup were sampled for a time interval of up to  $t^* \sim 300$ , i.e.  $t^* \sim 100$  greater than the  $t^* \sim 200$  reported in previous works<sup>18,19</sup>.

### 1. Effect of Fractal Dimension on Agglomerate Breakup

**Figure 5** shows the critical stress that the local hydrodynamic stress must overcome to restructure or breakup an agglomerate held together by van der Waals forces as a function of the number of primary particles in the agglomerate,  $N_{pp}$ , for four values of the fractal dimension,  $d_f$ . The factors influencing the critical stress, based on the empirical correlation in Eq. (7), are the number of primary particles in the agglomerate and the agglomerate fractal dimension. Interestingly, keeping  $N_{pp}$  constant and increasing  $d_f$  from a value of 2.0 to 3.0 results in larger values of  $\sigma_{cr}$ , signifying an increase in the difficulty of breaking up an agglomerate. Conversely, the agglomerate strength becomes weaker with an increase in  $N_{pp}$  for a given  $d_f$ . However, at higher value of the fractal dimension, e.g.  $d_f = 2.8$  and 3.0,  $\sigma_{cr}$  follows a trend almost independent of  $N_{pp}$ , especially at higher values of  $N_{pp}$ . The variation of  $\sigma_{cr} \sim f(d_f, N_{pp})$  therefore indicates that the fractal dimension and size of the agglomerate are key parameters that control

the breakup process, and that the fragmentation dynamics of an agglomerate become slower as the fractal dimension increases. On the balance of probability, it can be concluded that the influence of the fractal dimension of the agglomerate on agglomerate breakup is more significant than that of agglomerate size

30

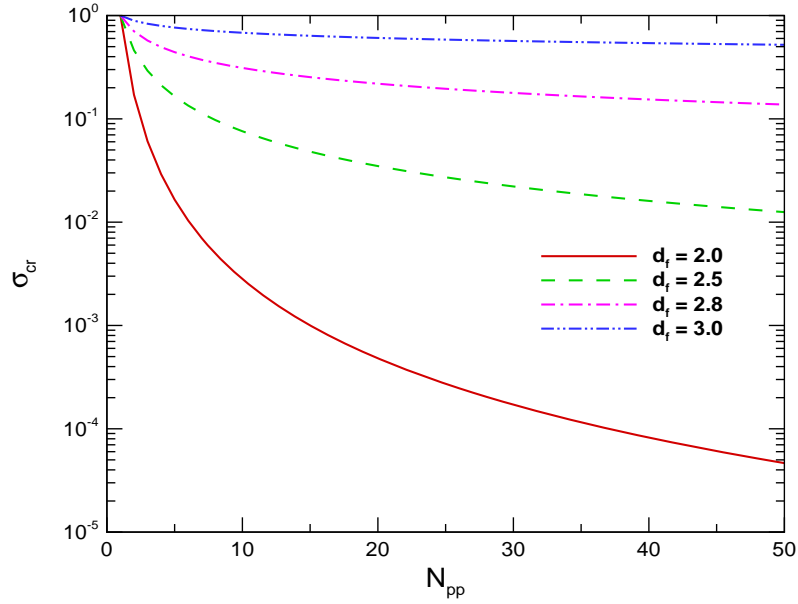


**Fig. 5:** Variation of agglomerate critical shear stress,  $\sigma_{cr}$ , as a function of number of primary particles in an agglomerate,  $N_{pp}$ , for a given agglomerate fractal dimension,  $2.0 \ll d_f \ll 3.0$ .

The effect of the fractal dimension on the location where breakup events occur, irrespective of the agglomerate type (or size) involved, is shown in the probability density functions,  $PDF(x^*)$ , in **Fig. 6**. With respect to the contours of the turbulence kinetic energy dissipation rate shown in **Fig. 2(b)**, it is evident in **Fig. 6** that the fractal dimension has a large effect on the probability of the location along the wall-normal direction,  $x^*$ , at which agglomerate breakup occurs. For a fractal dimension  $d_f = 2.0$ , **Fig. 6(a)** shows that agglomerate breakup occurs at all positions between the two parallel walls bounding the channel flow. Most of the breakup presented in **Fig. 6(a)** occurs in the near-wall regions. This observation is significantly different when compared to all other cases where  $d_f > 2.0$ . In relation to the agglomerate

critical stress,  $\sigma_{cr}$ , given in **Fig. 5**, the agglomerate strength is strongly dependent on  $d_f$ , hence, breakup occurs mostly in the near-wall regions where the hydrodynamic stress,  $\sigma \sim \epsilon^{1/2}$ , resulting from the local turbulence kinetic energy dissipation rate,  $\epsilon$ , is largest, as shown in the contours of **Fig. 2(b)**. For the  $d_f = 2.8$  and  $3.0$  cases, agglomerate breakup occurs at the plane closest to both walls where the stresses are at a maximum value.

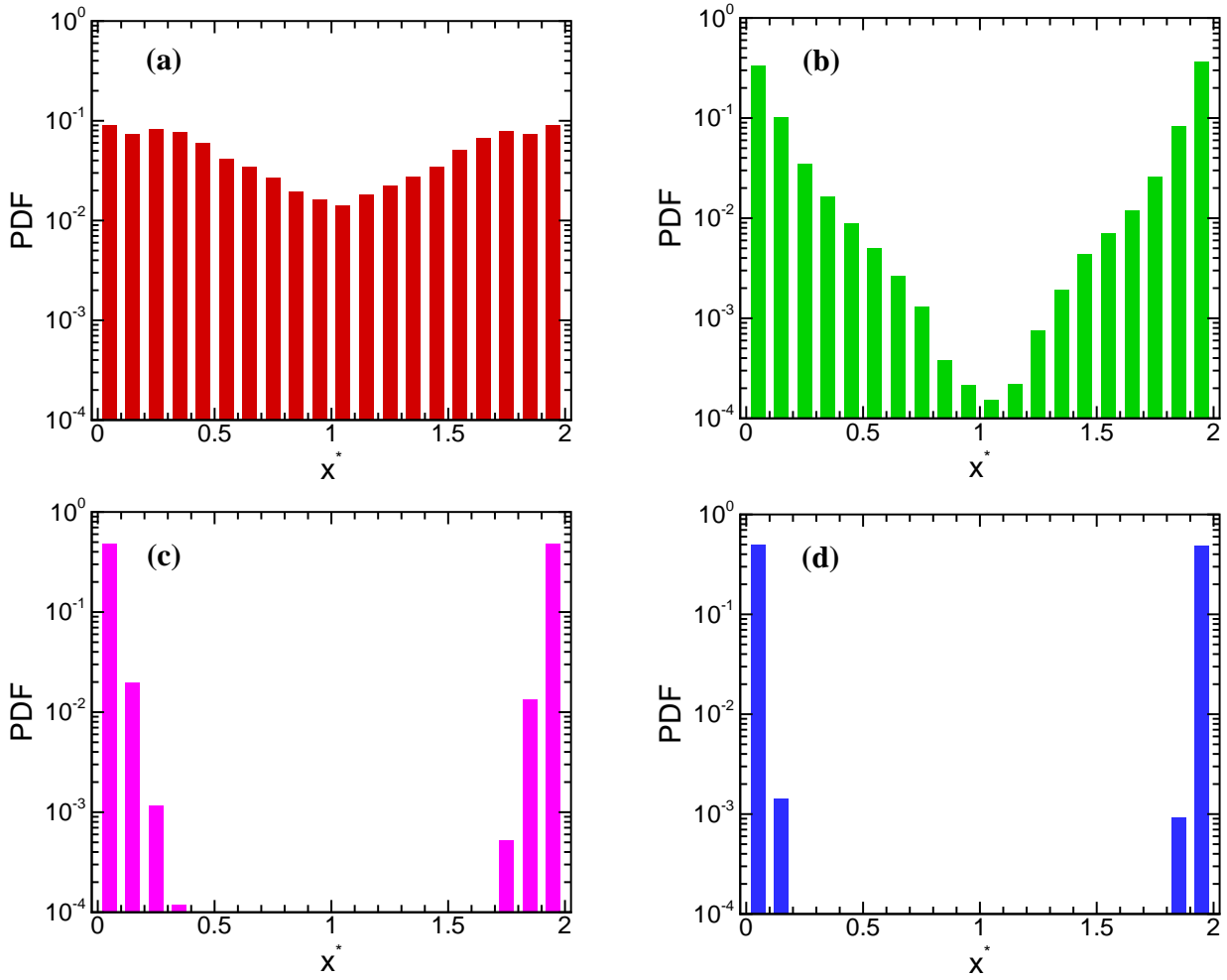


**Fig. 6:** Influence of fractal dimension,  $d_f$ , of the agglomerate structure on the probability density function,  $PDF(x^*)$ , of the non-dimensional position in the wall-normal direction where agglomerate breakup occurs.  $d_f =$  (a) 2.0, (b) 2.5, (c) 2.8 and (d) 3.0.

Overall, **Figs. 5** and **6** clearly show that the number of agglomerate breakup events increases as the agglomerate fractal dimension, a measure of the agglomerate strength, decreases, with a significant

difference between the two low strength ( $d_f = 2.0$  and  $2.5$ ) cases, shown in **Fig. 6(a)** and **(b)**, and the two high strength cases ( $d_f = 2.8$  and  $3.0$ ), shown in **Fig. 6(c)** and **(d)**. This observation is consistent with those reported in literature <sup>30</sup>.

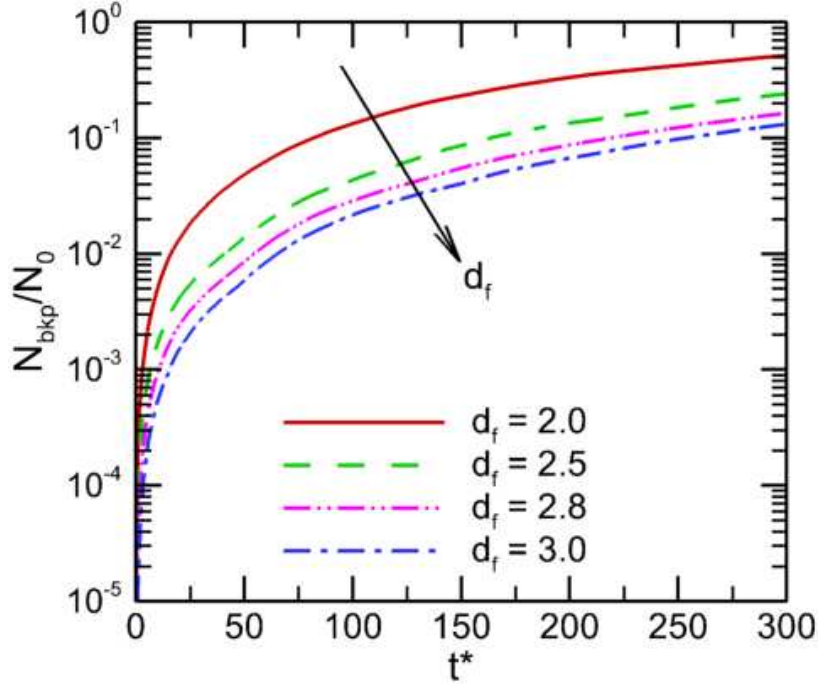


**Fig. 7:** Influence of fractal dimension,  $d_f$ , of the agglomerate structure on the time history of breakup events,  $N_{b_{kp}}$ , normalised by the initial number of primary particles,  $N_0$ .

The time evolution of the cumulative normalised number of agglomerate breakup events,  $N_{bk}/N_0$ , irrespective of the agglomerate type (or size), against the normalised time,  $t^*$ , is shown in a log-linear plot in **Fig. 7** for various agglomerate fractal dimensions. The results in **Fig. 7** show, as expected, that the number of breakup events decreases with increasing agglomerate fractal dimension from  $d_f = 2.0$  to  $3.0$ , and further confirms the findings reported in relation to the results of **Figs. 5** and **6**.

The influence of the agglomerate structure fractal dimension ( $d_f = 2.0, 2.5, 2.8$  and  $3.0$ ) on the total number of accumulated agglomerate breakup events,  $N_{b_{kp}}$ , of the same type (i.e. double (2), triple (3), quadruple (4), etc. particles) after a simulation time  $t^* = 300$  is shown in **Fig. 8**. The average number of

accumulated breakup events of any agglomerate type is highest for agglomerate type (2) and reduces as the agglomerate size increases up to type (20). This trend is to be expected as the primary event of agglomeration must occur first before the secondary event of breakup. The initial phase of particle pair formation, for all values of the fractal dimension, favours agglomerates of smaller sizes which are then subjected to breakup processes before undergoing subsequent phases of agglomeration. As will be shown later in **Fig. 13** which considers the temporal particle size distribution, the smaller agglomerates outnumber the larger agglomerate sizes. A large number of smaller sized agglomerates is a prerequisite for the large number of small agglomerate breakups, assuming favourable breakup conditions with reference to **Figs. 2, 5** and **6**. Hence, at any reference time,  $t^*$ , the agglomerates of smaller size first undergo breakup before the formation of larger agglomerates is possible for a given fractal dimension.

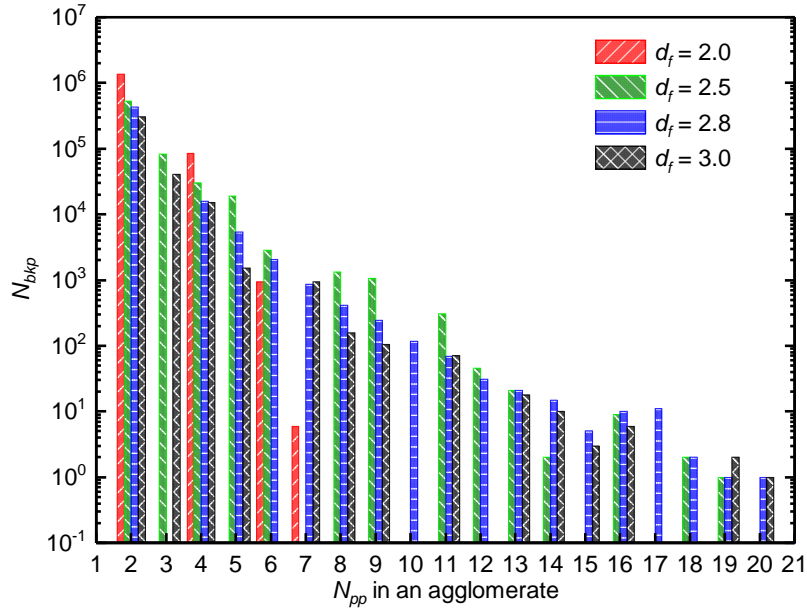


**Fig. 8:** Influence of fractal dimension,  $d_f$ , of the agglomerate structure on the number of agglomerates of the same type (double (2), triple (3), quadruple (4), etc. particles) that undergo breakup.

In addition, for each agglomerate type, e.g. double (2) agglomerates, the number of breakup events decreases as the fractal dimension increases from 2.0 to 3.0. This observation corroborates those made in relation to the results of **Fig. 5** where small values of  $d_f$  were noted to promote breakup. In the case of

particular fractal dimensions, no-breakup was recorded for agglomerates of the triple (3) type for  $d_f = 2.5$ , while type (7) was the largest agglomerate size to undergo breakup. For  $d_f = 2.5$ , agglomerates of type (7, 10, 15, 17 and 20) did not undergo breakup, whilst for  $d_f = 2.8$  and 3.0, all agglomerate types were involved in breakup apart from type (3), for  $d_f = 2.8$ , and for types (10 and 17), for  $d_f = 3.0$ . Further inspection of **Fig. 8** also suggests that breakup events for large values of the fractal dimension, i.e.  $d_f \geq 2.8$ , involve a wider spectrum of agglomerate types when compared to those with small values of the fractal dimensions, i.e.  $d_f \leq 2.5$ .

## 2. Effect of Fractal Dimension on Particle-Particle Interactions

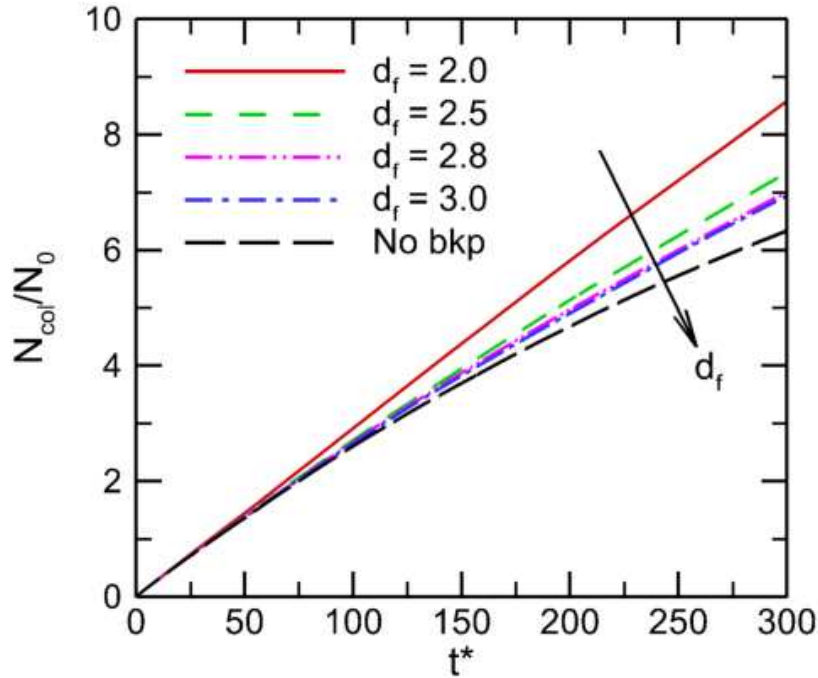


**Fig. 9:** Influence of fractal dimension,  $d_f$ , of the agglomerate structure on the time history of the number of collisions,  $N_{col}$ , normalised by the initial number of primary particles,  $N_0$ .

**Figure 9** shows the influence of the fractal dimension of the agglomerate structure on the total number of accumulated particle-particle collisions,  $N_{col}$ , normalised by the initial number of primary particles injected,  $N_0$ , as a function of time. These results show that breakup model with  $d_f = 2.0$  predicts the

largest number of particle-particle collisions, consistent with the breakup events mentioned in relation to **Figs. 6-8**. More collisions occur with decreasing fractal dimension from the limit case of no-breakup (*No bkp*) through  $d_f = 3.0$  to  $d_f = 2.0$ . It is obvious that the breaking up of an agglomerate in the flow populates it with smaller agglomerates containing a smaller number of primary particles which have a higher propensity to collision and subsequent agglomeration<sup>4, 18, 48</sup>. Hence, as most breakup occurs towards the end of the reported breakup time history in **Fig. 7**, its effect on the number of collisions in **Fig. 9** is more pronounced at high  $t^*$  than at earlier simulation times.

**Figure 10** shows the temporal development of the population of inter-particle collisions leading to agglomeration,  $N_{agg}/N_0$ , hereafter called agglomeration events, for four values of the fractal dimension and the no-breakup case. Similarly, the time history of the normalised total number of agglomerates,  $N_a/N_0$ , independent of their type (or size), as a function of time and as a consequence of particle agglomeration and breakup events is shown in **Fig. 11**. Similar to the relationship between  $N_{col}/N_0$  and  $d_f$ , the agglomeration events,  $N_{agg}/N_0$ , in **Fig. 10** decrease as  $d_f$  decreases from 2.0 to 3.0, with the lowest values occurring for the no-breakup case. The case with  $d_f = 2.0$  has the greatest number of agglomeration events consistent with the largest number of inter-particle collisions, as in **Fig. 9**, as well as the highest number of breakup events, as in **Fig. 7**. A high number of inter-particle collisions is a prerequisite for a large number of agglomeration processes, assuming that the sticking force is sufficiently large<sup>18</sup>, while breakup events populate the flow with agglomerates with fewer numbers of primary particles, a precursor to high collision rates<sup>4, 20</sup>.

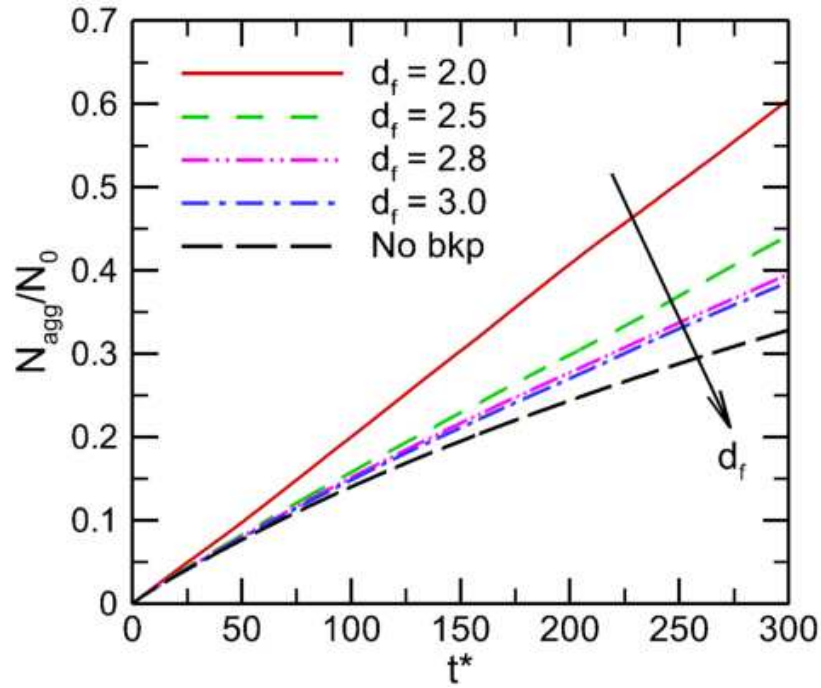


**Fig. 10:** Influence of fractal dimension,  $d_f$ , of the agglomerate structure on the time history of the total number of particle-particle collisions leading to agglomeration,  $N_{agg}$ , normalised by the initial number of primary particles,  $N_0$ .

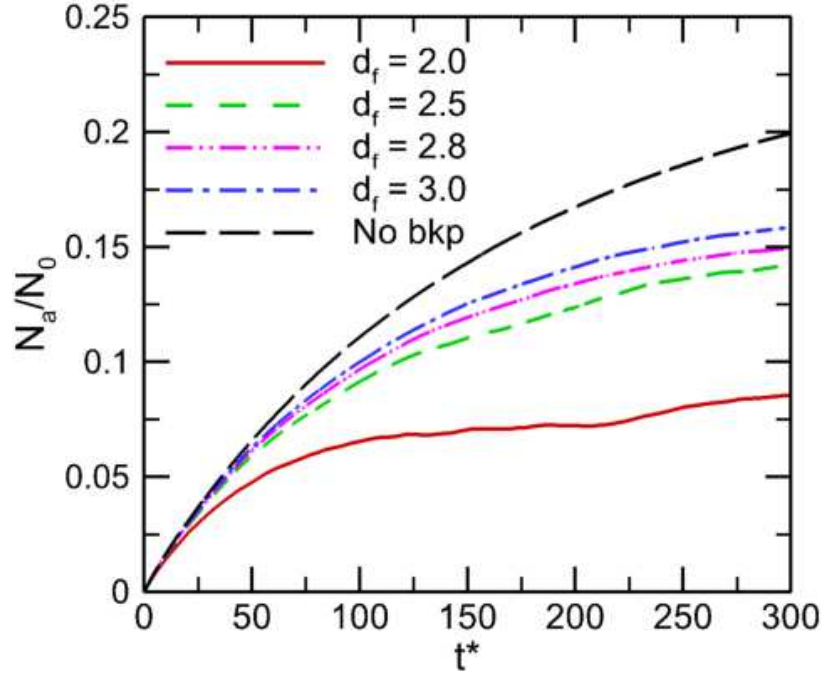


**Fig. 11:** Influence of fractal dimension,  $d_f$ , of the agglomerate structure on the time history of the total number of agglomerates,  $N_a$ , normalised by the initial number of primary particles,  $N_0$ .

In **Fig. 11**, a smaller fractal dimension, synonymous with a weaker agglomerate bonding strength, predicts a significant decrease in the number of agglomerates in the system with time. The results in **Fig. 7** indicate that agglomerates with smaller  $d_f$ , as in the case where  $d_f = 2.0$ , favour agglomerate breakup which then populate the flow with particles of relatively smaller size. Smaller particles which have higher surface areas have been shown to favour particle collision and agglomeration, and hence have higher agglomeration rates, as shown in **Fig. 12** and in previous works<sup>4, 18, 48</sup>. Subsequently, these smaller particles that evolved because of breakup events collide and re-agglomerate. Hence, this supports the results of **Fig. 9** where the case with  $d_f = 2.0$  exhibits the highest collision rates, and the results of **Fig. 10** where the same case shows the greatest cumulative number of agglomeration events. Note that the curve for  $d_f = 2.0$  in **Fig. 11**, as well as in **Figs. 12** and **13**, is not smooth when compared to the other fractal dimension cases. This is because for the former case, after the onset of agglomeration, the agglomeration process is in strong competition with the breakup process since, as noted in relation to **Figs. 5** and **6**, the agglomerates formed at  $d_f = 2.0$  are highly susceptible to breakup. Hence, the apparent equilibrium between the rates of agglomeration and breakup causes the small variations in  $N_a/N_0$  with time as agglomeration events are quickly undone by the breakup mechanism.

The results in **Fig. 11** show a strong dependency between  $d_f$  and the cumulative number of agglomerates present in the system at any time,  $N_a$ . Such behaviour is consistent with that observed by Soo *et al.*<sup>30</sup> who used a population balance equation method and found a strong dependency of agglomeration processes on the fractal dimension. As noted, this is consistent with  $N_{col}$  and  $N_{agg}$  in **Figs. 9** and **10**. As more agglomerates are broken up, the number of agglomerates in the system is depleted, leaving the number of agglomerates remaining to be lower at small  $d_f$  than at larger values. The difference in the number of agglomerates in the system for the various  $d_f$  values increases with time. Hence, in **Fig. 11** the case with  $d_f = 2.0$  results in smaller  $N_a/N_0$  values than for the case with  $d_f = 3.0$ . The no-breakup

case, as expected, shows the largest  $N_a/N_0$  values with time as all agglomerates are only consumed by forming larger structures and none are consumed in forming smaller agglomerate sizes.

**Figure 12** shows the accumulated collision efficiency (also known as the agglomeration rate),  $N_{agg}/N_{col}$ , defined as the ratio of the total number of accumulated particle-particle collisions leading to agglomeration to the total number of the accumulated particle-particle collisions, as a function of time for four values of the fractal dimension,  $d_f$ . It is clear that the largest agglomeration rate is predicted by the  $d_f = 2.0$  case, followed by the  $d_f = 2.5, 2.8, 3.0$  and the no-breakup cases.

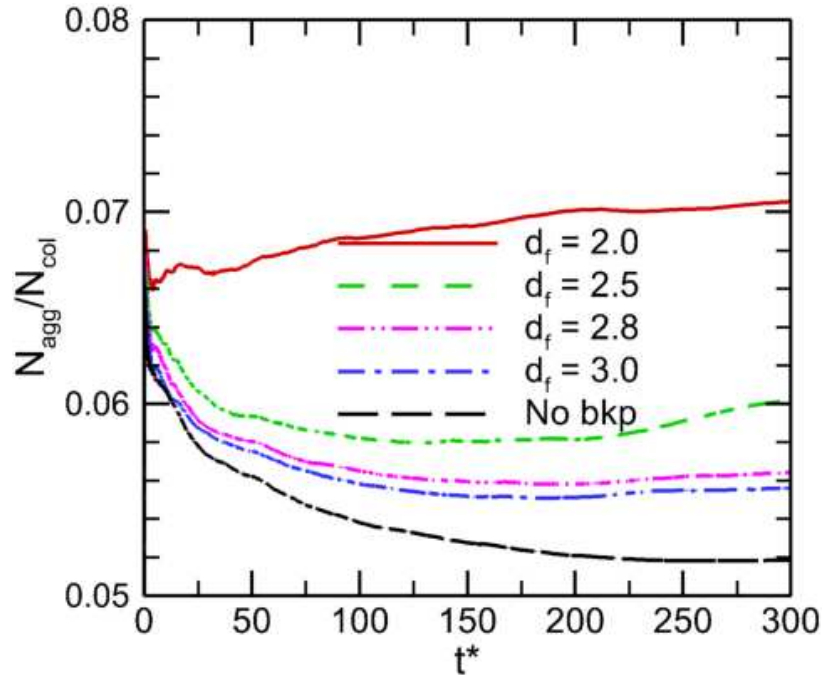


**Fig. 12:** Influence of fractal dimension,  $d_f$ , of the agglomerate structure on the time history of the agglomeration ratio rate, expressed as the inverse of the ratio of the total number of particle-particle collisions,  $N_{col}$ , to the total number of collisions leading to agglomeration,  $N_{agg}$ .

The rate of agglomerate formation starts at  $N_{agg}/N_{col} \sim 0.07$  and reduces at the same rate during the initial (pair-formation) phase for all the five breakup cases (no-breakup included). However, as time progresses into the breakup phase of the newly formed agglomerates and the cluster-cluster agglomeration phase, the agglomeration rate of the  $d_f = 2.0$  case reverses from decreasing to steadily increasing with

time. At the same time, the agglomeration rate for the other cases ( $d_f = 2.5 - 3.0$ , and  $d_f \rightarrow \infty$ ) continues to decrease with time. This decrease is maintained until at about  $t^* \sim 100$  when it shifts to an increasing trend with time when the breakup process for the  $d_f = 2.5, 2.8$  and  $3.0$  cases has increased significantly due to the availability of agglomerates of larger sizes. During this time, the base case of no-breakup maintains the previously observed agglomeration rate – time relationship<sup>4, 18-20, 48</sup>, i.e. in cases where appropriate initial conditions for the particle-particle interactions and no agglomerate breakup are considered, the agglomerate rate has been reported<sup>4, 18-20, 48</sup> to reduce with time. Overall, the value of the agglomeration rate decreases significantly when increasing the fractal dimension from  $d_f = 2.0$  through  $d_f = 3.0$  to the no-breakup case. Similar behaviour, with a strong dependency of the agglomeration process on the fractal dimension, was also observed in Soo *et al.*<sup>30</sup> where for fractal dimension  $d_f = 1.8$  the initial dynamics of the moment ratio was significantly different from all other cases with  $d_f > 1.8$ . This behaviour is attributed to the fact that at a very small fractal dimension, e.g.  $d_f \leq 2.0$ , the agglomerate structure is so weak that the agglomerate undergoes breakup easily, hence, populating the system with particles of smaller sizes. These smaller sized particles are subsequently susceptible to collision and agglomeration, having a higher agglomeration rate than cases with a larger fractal dimension,  $d_f > 2.0$ . In addition, as shown in Fig. 5 and in Eq. (7), the relationship between agglomerate breakup and fractal dimension is not linear but a power function. Hence, there is a large difference in breakup processes occurring at lower and higher  $d_f$ .

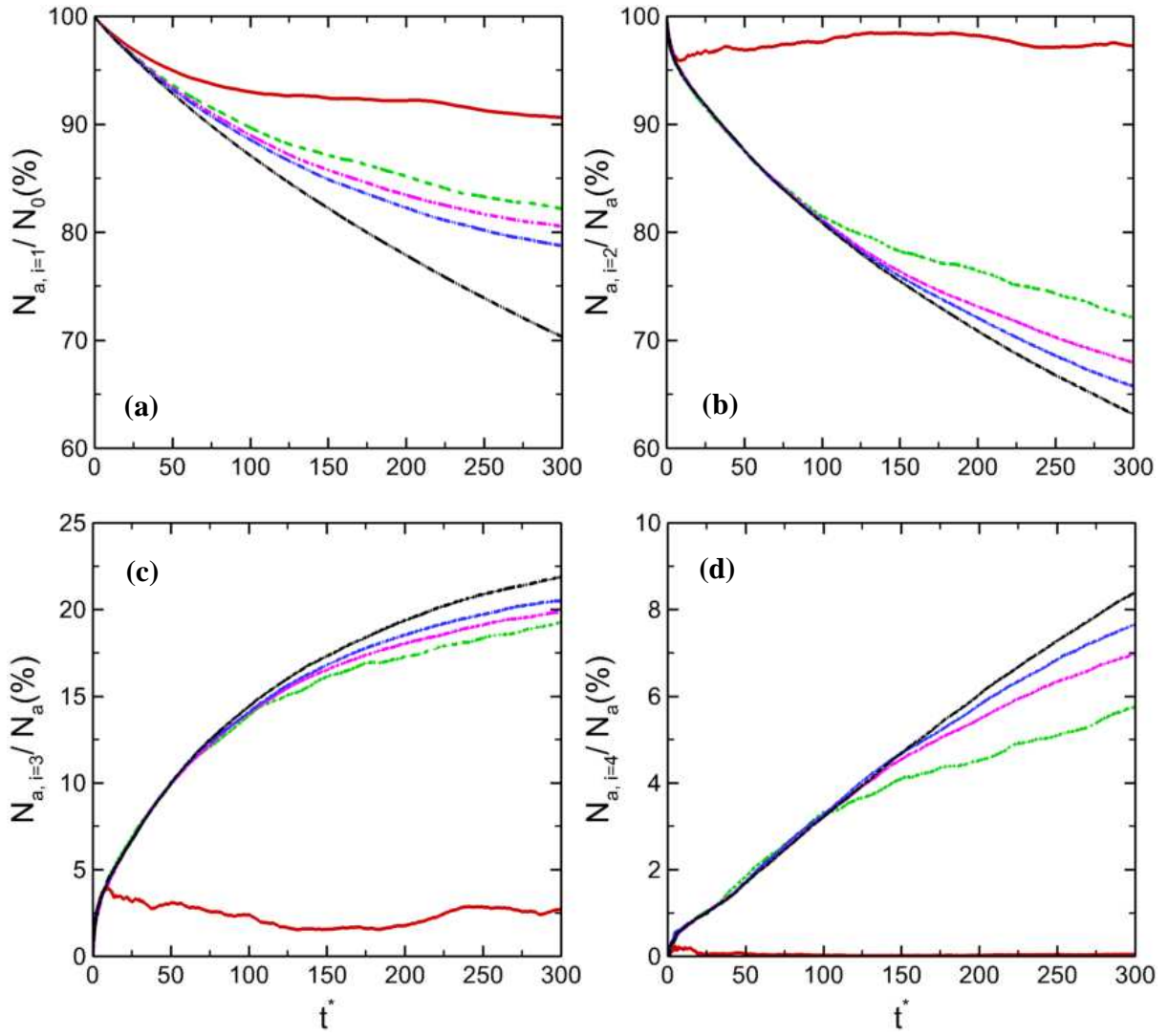


**Fig. 13:** Influence of fractal dimension,  $d_f$ , of the agglomerate structure on the time history of the particle size distribution,  $N_{a,i}$ , expressed as: (a) a percentage of the evolution of the primary particle size,  $N_{a,i=1}$ , normalised by the initial number of primary particles,  $N_0$ , and (b, c, d) a percentage of the population of agglomerate size,  $N_{a,i>1}$ , normalised by the total number of agglomerates present,  $N_a$ . Key as Fig. 12.

The transient particle size distribution, with the primary particles (single(1)),  $N_{a,i=1}$ , presented as a percentage of the initial number of all primary particle,  $N_0$ , and the agglomerates (double (2), triple (3), etc),  $N_{a,i>1}$ , presented as a percentage of the total number of all agglomerates,  $N_a$ , with time,  $t^*$ , is shown in **Fig. 13** for all breakup cases considered. For the population of single particles in **Fig. 13(a)**, the profiles start at 100% when the system is populated by only the  $N_{a,i=1}$  sized single particles. Then as time

progresses and the pair-formation and cluster-cluster formation phases set in, more of the  $N_{a,i=1}$  particles are consumed leading to a steady reduction in the number of these particles with time. However, as the system progresses further into the breakup phase, the population balance of the  $N_{a,i=1}$  sized single particles predicted by the  $d_f = 2.0$  case starts increasing with time until the profile flattens out at a steady level of about 90%. At this point there seems to be a pseudo-equilibrium between the rate of consumption of the  $N_{a,i=1}$  sized particles in the production of agglomerates and the rate of their replenishment due to the breakup of agglomerates. Contrary to the behaviour of the  $d_f = 2.0$  case, the other cases,  $d_f > 2.0$ , continue to reduce with time, with the reduction rate inversely proportional to the strength of the agglomerate, and with the base case of no-breakup showing about 70% of the  $N_{a,i=1}$  particles remaining at  $t^* = 300$ .

For the population balance of the agglomerates,  $N_{a,i \geq 2}$ , shown in **Fig. 13**, it follows that the rate of consumption of the double (2) particles in **Fig. 13(b)**, triple (3) in **Fig. 13(c)** and quadruple (4) in **Fig. 13(d)** in the production of larger sized agglomerates, and the rate of replacement of the agglomerate type due to breakup, are identical for the weakest agglomerate structure case, i.e. for  $d_f = 2.0$ . The percentage of the agglomerate for the  $d_f = 2.0$  case stabilises at approximately 97%, 2.5% and 0% for the  $N_{a,i=2}$ ,  $N_{a,i=3}$  and  $N_{a,i=4}$  cases, respectively. However, for the other  $d_f > 2.0$  cases, the relationship between the rate of production of a specific agglomerate size and its corresponding consumption varies depending on the agglomerate size. In the case of double-sized agglomerates,  $N_{a,i=2}$ , their population steadily reduces with time, with the no-breakup case giving the lowest values. This is because for this agglomerate only depletion due to agglomeration occurs, with no-breakup of larger particles balancing the consequent reduction in their number. For the larger agglomerate sizes,  $N_{a,i=3}$  and  $N_{a,i=4}$ , their population increases with time since their number is skewed towards production rather than depletion by either breakup or agglomeration.

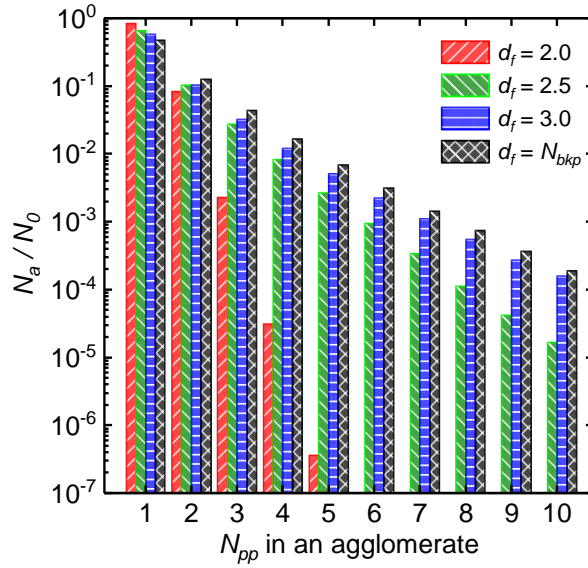


**Fig. 14:** Influence of fractal dimension,  $d_f$ , of the agglomerate structure on the time history of the particle size distribution,  $N_{a,i}$ , expressed as: (a) a percentage of the evolution of the primary particle size,  $N_{a,i=1}$ , normalised by the initial number of primary particles,  $N_0$ , and (b, c, d) a percentage of the population of the agglomerate size,  $N_{a,i>1}$ , normalised by the total number of agglomerate present,  $N_a$ .

Lastly, **Fig. 14** compares the number of primary particles (i.e. single (1)) and agglomerates of the same type (double (2), triple (3), quadruple (4), quintuple (5), sextuple (6), etc. particles) existing at simulation time  $t^* = 300$  for the four fractal dimension ( $d_f = 2.0, 2.5, 2.8$  and  $3.0$ ) and the no-breakup base case. Note that only up to  $N_{pp} = 10$  agglomerate sizes are shown even though larger sizes were observed in the simulation. The results shown complement the findings noted in relation to **Fig. 13** where the number of a specific particle size decreases as the particle size increases. Hence, the number of the single particles is larger than the number of double, triple, etc. particles, and so on. For the single particles, the number remaining at  $t^* = 300$  predicted for the  $d_f = 2.0$  case is larger than for the other cases, and an inverse relationship between their number and the value of  $d_f$  is maintained. However, the reverse is the case for the number of agglomerates sizes,  $N_{pp}$ , computed with respect to  $d_f$ . **Figure 14** therefore indicates that the number of a specific size of agglomerate remaining in the system increases with an increase in the value of  $d_f$ , with an approximately linear relationship between the remaining  $N_{pp}$  particles and  $d_f$ . The

base no-breakup case shows the largest number of agglomerate sizes remaining in the system, with up to  $N_{pp} = 10$ . The strength of the agglomerate is characterised by the fractal dimension,  $d_f$ , and the size of the agglomerate,  $N_{pp}$ , as  $\sigma_{cr} \sim f(d_f, N_{pp})$ . Hence, as the agglomerate size increases, the strength of the agglomerate becomes weaker and it is more susceptible to breakup. Therefore, at smaller  $d_f$  and larger  $N_{pp}$ , more agglomerates will breakup, thereby depleting the number of such large agglomerate types. This is evidenced by the  $d_f = 2.0$  case where only a small number of  $N_{pp} = 5$  particles remain in the system at  $t^* = 300$ .

## V. CONCLUSIONS

Following preliminary results of turbulence-induced particle agglomeration and breakup presented recently<sup>49</sup>, large eddy and discrete particle simulation have been used to predict particle agglomeration and breakup processes, together with a deterministic treatment of inter-particle collisions and particle feedback effects on the fluid phase. Agglomeration is based on the pre-collision energy-momentum balance, restitution coefficient and van der Waals interactions. To allow the overall model to be applied to practical processes, it was also extended to handle the breakup of the agglomerates. Agglomerate breakup was considered to occur instantaneously subject to a hydrodynamic stress exceeding a critical value dictated by the properties of the agglomerate. In terms of the critical stress that must be overcome for breakup to occur, the fractal dimension and size of the agglomerate are key parameters that control the process, with the fragmentation dynamics of an agglomerate becoming slower as the fractal dimension increases. Breakup events also increase with time as larger agglomerates are formed which are weaker in strength and hence susceptible to breakup. Breakup events, therefore, reduce the number of agglomerates in the system as well as populating it with particles of smaller size, thereby promoting more collisions and collisions leading to agglomeration. Predictions for the base case of no-breakup followed the behaviour previously reported in literature<sup>4, 18-20, 48</sup>.

For agglomerates of low strength ( $d_f = 2.0$  and  $2.5$ ), breakup was found to occur at all locations between the two walls of a turbulent channel flow, but mostly in the near-wall regions where the local hydrodynamic stresses,  $\sigma \sim \epsilon^{1/2}$ , resulting from the local turbulence kinetic energy dissipation rate,  $\epsilon$ , are greatest. For higher strength agglomerates ( $d_f = 2.8$  and  $3.0$ ), agglomerate breakup occurred at the plane closest to both walls where the stresses are at a maximum value.

These results support the conclusion that the local energy dissipation rate controls the kinetics of the agglomerate breakup process while the kinetic energy controls the agglomeration processes itself which occurs mostly in the bulk region of the channel flow. The bulk flow assists the transportation of the agglomerates towards the high shear stress regions where they experience high dissipation rates and break as a consequence.

The predictive technique developed and demonstrated provides a powerful simulation tool which is fundamental and generic in nature, and which can be applied to particle agglomeration and agglomerate breakup under aerodynamic and hydrodynamic conditions that occur in many industrial and natural processes. Finally, it should be noted that for validation of the techniques reported there is a requirement for relevant detailed experimental data which are at present scarce, notwithstanding the obvious difficulties inherent in measuring the processes of interest.

## **VI. ACKNOWLEDGEMENTS**

The authors would like to thank Innovate UK for their financial support of the work described under grant 167248, “Measurement and Modelling of Sludge Transport and Separation Processes” and the EPSRC for their support of the DISTINCTIVE (Decommissioning, Immobilisation and Storage Solutions for Nuclear Waste Inventories) Consortium under grant EP/L014041/1. The authors gratefully acknowledge the useful discussions held with other colleagues, in particular Kevin Malone and Darren Edgar of MMI Engineering, Geoff Randall and Martyn Barnes of Sellafield Ltd, and Timothy Hunter and

David Harbottle of the School of Chemical and Process Engineering. Part of this work was undertaken on ARC2 and ARC3, part of the high performance computing facilities at the University of Leeds.

## VII. REFERENCES

1. J. Pozorski, "Models of turbulent flows and particle dynamics", in: J.-P. Minier, J. Pozorski J. (eds), *Particles in Wall-Bounded Turbulent Flows: Deposition, Re-Suspension and Agglomeration*, CISM International Centre for Mechanical Sciences, Vol. 571 (Springer, Cham, 2017).
2. D.O. Njobuenwu, M. Fairweather, and J. Yao, "Coupled RANS-LPT modelling of dilute, particle-laden flow in a duct with a 90° bend," *Int. J. Multiphase Flow* **50**, 71 (2013).
3. B. Rosa, and L.-P. Wang, "Parallel implementation of particle tracking and collision in a turbulent flow", in: R. Wyrzykowski, J. Dongarra, K. Karczewski, J. Wasniewski (eds), *Parallel Processing and Applied Mathematics*, Vol 6068 (Springer, Berlin, Heidelberg, 2010).
4. D.O. Njobuenwu, and M. Fairweather, "Simulation of deterministic energy-balance particle agglomeration in turbulent liquid-solid flows," *Phys. Fluids* **29**, 083301 (2017).
5. M.W. Reeks, "Transport, mixing and agglomeration of particles in turbulent flows," *Flow Turbul. Combust.* **92**, 3 (2014).
6. G. Falkovich, A. Fouxon, and M. G. Stepanov, "Acceleration of rain initiation by cloud turbulence," *Nature* **419**, 151 (2002).
7. D.R. Rector, and B.C. Bunker, "Effect of colloidal aggregation on the sedimentation and rheological properties of tank waste", Pacific Northwest Laboratory, Report No. PNL-10761, 1995.
8. C. Marchioli, and A. Soldati, "Mechanisms for particle transfer and segregation in a turbulent boundary layer," *J. Fluid Mech.* **468**, 283 (2002).
9. D.G.E. Grigoriadis, and S.C. Kassinos, "Lagrangian particle dispersion in turbulent flow over a wall mounted obstacle," *Int. J. Heat Fluid Flow* **30**, 462 (2009).
10. H. Huang, X. Yang, M. Krafczyk, and X.-Y. Lu, "Rotation of spheroidal particles in Couette flows," *J. Fluid Mech.* **692**, 369 (2012).
11. L. Zhao, C. Marchioli, and H.I. Andersson, "Slip velocity of rigid fibers in turbulent channel flow," *Phys. Fluids* **26**, 063302 (2014).
12. S. Sundaram, and L.R. Collins, "Collision statistics in an isotropic particle-laden turbulent suspension. Part 1. Direct numerical simulations," *J. Fluid Mech.* **335**, 75 (1997).
13. M. Lee, and R.D. Moser, "Direct numerical simulation of turbulent channel flow up to  $Re_\tau=5200$ ," *J. Fluid Mech.* **774**, 395 (2015).

14. K.C.J. Schutte, L.M. Portela, A. Twerda, and R.A.W.M. Henkes, "Hydrodynamic perspective on asphaltene agglomeration and deposition," *Energy Fuels* **29**, 2754 (2015).
15. B.P.B. Hoomans, J.A.M. Kuipers, W.J. Briels, and W.P.M. van Swaaij, "Discrete particle simulation of bubble and slug formation in a two-dimensional gas-fluidised bed: A hard-sphere approach," *Chem. Eng. Sci.* **51**, 99 (1996).
16. M. Chen, K. Kontomaris, and J.B. McLaughlin, "Direct numerical simulation of droplet collisions in a turbulent channel flow. Part I: collision algorithm," *Int. J. Multiphase Flow* **24**, 1079 (1999).
17. Y. Yamamoto, M. Potthoff, T. Tanaka, T. Kajishima, and Y. Tsuji, "Large-eddy simulation of turbulent gas-particle flow in a vertical channel: effect of considering inter-particle collisions," *J. Fluid Mech.* **442**, 303 (2001).
18. M. Breuer, and N. Almohammed, "Modeling and simulation of particle agglomeration in turbulent flows using a hard-sphere model with deterministic collision detection and enhanced structure models," *Int. J. Multiphase Flow* **73**, 171 (2015).
19. N. Almohammed, and M. Breuer, "Modeling and simulation of agglomeration in turbulent particle-laden flows: A comparison between energy-based and momentum-based agglomeration models," *Powder Technol.* **294**, 373 (2016).
20. D.O. Njobuenwu, and M. Fairweather, "Deterministic modelling of particle agglomeration in turbulent flow", in: K. Hanjalic, T. Miyauchi, D. Borello, M. Hadziabdic, P. Venturini, P. (eds), *Proceedings of the Eighth International Symposium on Turbulence, Heat and Mass Transfer* (Begell House Inc., New York, 2015).
21. M. Afkhami, A. Hassanpour, M. Fairweather, and D.O. Njobuenwu, "Fully coupled LES-DEM of particle interaction and agglomeration in a turbulent channel flow," *Comput. Chem. Eng.* **78**, 24 (2015).
22. A.S. Hellestø, M. Ghaffari, B.V. Balakin, and A.C. Hoffmann, "A parametric study of cohesive particle agglomeration in a shear flow – numerical simulations by the discrete element method," *J. Dispersion Sci. Technol.* **38**, 611 (2017).
23. P.A. Cundall, and O.D.L. Strack, "A discrete numerical model for granular assemblies," *Géotechnique* **29**, 47 (1979).
24. C.A. Ho, and M. Sommerfeld, "Modelling of micro-particle agglomeration in turbulent flows," *Chem. Eng. Sci.* **57**, 3073 (2002).
25. M. Sommerfeld, and S. Stübing, "A novel Lagrangian agglomerate structure model," *Powder Technol.* **319**, 34 (2017).
26. M. Sommerfeld, "Validation of a stochastic Lagrangian modelling approach for inter-particle collisions in homogeneous isotropic turbulence," *Int. J. Multiphase Flow* **27**, 1829 (2001).
27. Y. Ammar, A. Dehbi, and M.W. Reeks, "Break-up of aerosol agglomerates in highly turbulent gas flow," *Flow Turbul. Combust.* **89**, 465 (2012).

28. R. Wengeler, and H. Nirschl, "Turbulent hydrodynamic stress induced dispersion and fragmentation of nanoscale agglomerates," *J. Colloid Interface Sci.* **306**, 262 (2007).
29. M.U. Babler, L. Biferale, L. Brandt, U. Feudel, K. Guseva, A.S. Lanotte, C. Marchioli, F. Picano, G. Sardina, A. Soldati, and F. Toschi, "Numerical simulations of aggregate breakup in bounded and unbounded turbulent flows," *J. Fluid Mech.* **766**, 104 (2015).
30. M. Soos, J. Sefcik, and M. Morbidelli, "Investigation of aggregation, breakage and restructuring kinetics of colloidal dispersions in turbulent flows by population balance modeling and static light scattering," *Chem. Eng. Sci.* **61**, 2349 (2006).
31. M.L. Eggersdorfer, and S.E. Pratsinis, "The structure of agglomerates consisting of polydisperse particles," *Aerosol Sci. Technol.* **46**, 347 (2012).
32. G. Inci, A. Kronenburg, R. Weeber, and D. Pflüger, "Langevin dynamics simulation of transport and aggregation of soot nano-particles in turbulent flows," *Flow Turbul. Combust.* **98**, 1065 (2017).
33. M.U. Babler, L. Biferale, and A.S. Lanotte, "Breakup of small aggregates driven by turbulent hydrodynamical stress," *Phys. Rev. E* **85**, 025301 (2012).
34. C. Marchioli, and A. Soldati, "Turbulent breakage of ductile aggregates," *Phys. Rev. E* **91**, 053003 (2015).
35. C. Henry, J.-P. Minier, J. Pozorski, and G. Lefèvre, "A new stochastic approach for the simulation of agglomeration between colloidal particles," *Langmuir* **29**, 13694 (2013).
36. M. Bini, and W.P. Jones, "Particle acceleration in turbulent flows: A class of nonlinear stochastic models for intermittency," *Phys. Fluids* **19**, 035104 (2007).
37. A. Zaccone, M. Soos, M. Lattuada, H. Wu, M.U. Bäbler, and M. Morbidelli, "Breakup of dense colloidal aggregates under hydrodynamic stresses," *Phys. Rev. E* **79**, 061401 (2009).
38. M. Germano, U. Piomelli, P. Moin, and W.H. Cabot, "A dynamic subgrid-scale eddy viscosity model," *Phys. Fluids A* **3**, 1760 (1991).
39. U. Piomelli, and J. Liu, "Large-eddy simulation of rotating channel flows using a localized dynamic model," *Phys. Fluids* **7**, 839 (1995).
40. R. Mei, "An approximate expression for the shear lift force on a spherical particle at finite reynolds number," *Int. J. Multiphase Flow* **18**, 145 (1992).
41. W.P. Jones, F. di Mare, and A.J. Marquis, "LES-BOFFIN: Users guide", Technical Memorandum (Mechanical Engineering Dep't, Imperial College of Science, Technology and Medicine, London, UK, 2002).
42. M. Bini, and W.P. Jones, "Large-eddy simulation of particle-laden turbulent flows," *J. Fluid Mech.* **614**, 207 (2008).

43. D.O. Njobuenwu, and M. Fairweather, "Simulation of inertial fibre orientation in turbulent flow," *Phys. Fluids* **28**, 063307 (2016).
44. C. Marchioli, and A. Soldati, "Reynolds number scaling of particle preferential concentration in turbulent channel flow", in: J. Palma A.S. Lopes (eds), *Advances in Turbulence XI, Springer Proceedings Physics, Vol 117*. (Springer, Berlin, Heidelberg, 2007).
45. R.D. Moser, J. Kim, and N.N. Mansour, "Direct numerical simulation of turbulent channel flow up to  $Re_\tau=590$ ," *Phys. Fluids* **11**, 943 (1999).
46. J. Tomas, "Adhesion of ultrafine particles - A micromechanical approach," *Chem. Eng. Sci.* **62**, 1997 (2007).
47. C. Marchioli, A. Soldati, J.G.M. Kuerten, B. Arcen, A. Tanière, G. Goldensoph, K.D. Squires, M.F. Cargnelutti, and L.M. Portela, "Statistics of particle dispersion in direct numerical simulations of wall-bounded turbulence: Results of an international collaborative benchmark test," *Int. J. Multiphase Flow* **34**, 879 (2008).
48. B. Balakin, A.C. Hoffmann, and P. Kosinski, "The collision efficiency in a shear flow," *Chem. Eng. Sci.* **68**, 305 (2012).
49. D.O. Njobuenwu, and M. Fairweather, "Large eddy simulation of particle-particle interactions in turbulent flow: collision, agglomeration and break-up events," *Proceedings 11<sup>th</sup> International ERCOFTAC Symposium on Engineering Turbulence Modelling and Measurements*, 21-23 Sep 2016, Palermo, Italy.